Textile & Leather Review

ISSN 2623-6281 | www.tlr-journal.com | 10.31881/TLR

A New Synthesis Method and Characterization of Graphene Oxide Nanocomposites for the Leather Tanning Process

Shimul Chakma, Pronay Biswas, Md. Abdulla-Al-Mamun, Md. Abdul Mottalib, Fariha Chowdhury, Md. Abdul Goni

How to cite: Chakma S, Biswas P, Abdulla-Al-Mamun M, Mottalib MA, Chowdhury F, Goni MA. A New Synthesis Method and Characterization of Graphene Oxide Nanocomposites for the Leather Tanning Process. Textile & Leather Review. 2024; 7:738-769.
https://doi.org/10.31881/TLR.2024.036

How to link: https://doi.org/10.31881/TLR.2024.036

Published: 16 May 2024

A New Synthesis Method and Characterization of Graphene Oxide Nanocomposites for the Leather Tanning Process

Shimul CHAKMA[1], Pronay BISWAS[2], Md. ABDULLA-AL-MAMUN[2], Md. Abdul MOTTALIB[2*], Fariha CHOWDHURY[3], Md. Abdul GONI[4]

[1]Leather Research Institute, Bangladesh Council of Scientific and Industrial Research, Dhaka, Bangladesh

[2]Institute of Leather Engineering and Technology, University of Dhaka, Dhaka, Bangladesh

[3]Biomedical and Toxicological Research Institute, Bangladesh Council of Scientific and Industrial Research, Dhaka, Bangladesh

[4]Department of Biological and Physical Sciences, South Carolina State University, Orangeburg, USA

*abdul.mottalib@du.ac.bd

Article

https://doi.org/10.31881/TLR.2024.036

Received 29 February 2024; Accepted 29 April 2024; Published 16 May 2024

ABSTRACT

Environmental pollution caused by wastes generated from chrome tan is a major concern nowadays. This study aimed to develop an eco-friendly alternative tanning agent using graphene oxide (GO) based nanocomposite materials. GO was synthesized by a new approach with modification of the Hummers method. Two types of GO-based nanocomposites, GO-TiO_2 (GT) and GO-TiO_2-PEG (GTP) were prepared by adding TiO_2 nanoparticles and polyethylene glycol (PEG) as surface modifiers. They were successfully applied to leather tanning processes at different concentrations (2%, 4%, and 6%). Both synthesized GO, GO-nanocomposites, and the resulting tanned leathers were characterized by Scanning Electron Microscopy (SEM), Thermogravimetric Analysis (TGA), and Fourier-transform Infrared Spectroscopy (FT-IR). Different physico-mechanical properties of leathers tanned with nanocomposites were evaluated and the results were compared with chrome-tanned leathers. The tensile strength of chrome-tanned leather was 223 (kg/cm) whereas the maximum tensile strength was found at 228 (kg/cm) and 233 (kg/cm) in 6% GO-TiO_2 and GO-TiO_2-PEG tanned leathers respectively. The environmental pollution impact of the effluents generated by the new tanning process was assessed. The COD of effluents generated from chrome tanning was 4800 ppm which was significantly reduced to 2400-1440 ppm and 2880-1920 ppm when GO-TiO_2 (GT) and GO-TiO_2-PEG (GTP) were applied in leather tanning respectively. The TDS and BOD were found at 183.8 and 200 ppm in conventional chrome-tanned wastewater which were significantly reduced to the range of 47.5-18.3 and 100-50 ppm respectively in liquid wastes obtained from the GO-composite tanning process. The maximum reduction of COD, BOD, TDS, and TSS in leather waste liquid was found with the application of 2% GO-nanocomposites in tanning. The results revealed that leathers tanned with nanocomposites possess characteristic properties which were very similar to those observed in chrome-tanned leathers whereas the new tanning agents drastically reduced the intensity of pollutants in leather effluents. The application of new nanocomposites in the leather tanning process is an innovative effort. This new nanocomposite-tanning method showed minimal consequences regarding environmental pollution with the generation of less toxic effluents from the respective tanning process.

KEYWORDS

graphene oxide, nanocomposites, leather, tanning, synthesis, effluent, environment

INTRODUCTION

Chrome-tanning is a widely used technique in raw leather processing which contributes to 90% of the global leather supply [1]. This chrome tanning method emerged as quicker and more cost-effective in comparison to the traditional vegetable tanning process during the Industrial Revolution. Trivalent basic chromium sulfate, or $Cr(OH)SO_4$, solutions are commonly used in tanning operations conducted in different tannery industries. However, only about 60-70% of the applied chromium compounds react with collagen fibres throughout the tanning process and the rest remain unchanged and are being released from industries as tannery effluents [2,3]. Discharge of tannery wastewater without any chemical treatments or with partial treatment to the surrounding environment causes severe contamination in air, soil, surface and groundwater bodies in the respective areas which pose health risks to workers and other people in communities [4-7]. Chrome tanning causes serious environmental pollution as the process consumes as well as releases large quantities of inorganic chemicals in raw leather processing [8]. Uncontrol dumping of tannery wastes causes the distribution of toxic chromium (VI) species in the surrounding environment which severely contaminates soil, waterbodies and other components in terrestrial environments [9]. The trace quantity of Cr(III) is considered an essential element which plays an important role in the biochemical metabolism process, especially for diabetic patients [10]. However, the presence of a trace amount of Cr(VI) is extremely toxic and harmful to living organisms. Chromium pollution can cause a variety of serious health issues in humans working in tanning industries which include skin allergies, anaemia, kidney dysfunction, liver failure, lung disease, diarrhoea, vomiting, and situations that can produce mutagenic carcinogens [11]. Chromium toxicity in living species can occur in both acute and chronic ways [12] which may cause lung cancer [13]. Though Cr (III) sulfate is used in the raw leather manufacturing process, a significant amount of Cr (VI) is produced as a result of the oxidation of Cr (III) species during tanning operations. Application of unsaturated lipids and vegetable oils in the fatliquoring process may cause the oxidation of Cr (III) to Cr (VI) [3]. Moreover, exposure to UV light, a dry atmosphere, and high temperatures in the tanning process may also facilitate the oxidation of Cr (III) into Cr (VI) in the respective system [14]. Hexavalent chromium species was found in the wet finishing process especially under certain conditions [15]. It has been observed that the application of chrome tanning in leather industries posed a substantial threat of pollution in terrestrial environments as this tanning method showed a poor chromium ion absorption rate in leather processing steps. The unreduced dichromate species found in cationic chrome liquor may also contribute to an increase in the presence of Cr (VI) in chrome wastewater [11]. Due to the severe environmental and potential health risks caused by chromium-containing wastes, many researchers have worked on removing toxic chromium species from tannery wastewater bodies [16-19]. To keep our environment safe from pollution and to reduce health risks for workers in tannery industries, many attempts were made to avoid the application of chromium compounds in tanning

processes. Different alternative tanning materials such as vegetable tannins, oils, aldehyde tannins, zirconium tannins, aluminium tannins, titanium tannins, polymer tannins, amino acids, etc., were used in tanning operations [20-22]. However, these alternating tanning agents showed many limitations in tanning processes and they did not work effectively like chromium compounds thus the entire replacement of chromium with a viable alternative material was not found to be feasible in tannery industries [22]. Hence, there is an urgent need to design tanning chemicals that require minimal dosages and exhibit high usage efficiency in tanning processes or pre-treatment methods that can enhance the exhaustion of chromium species and thus fix the chrome tan issues [4,23]. Different nanomaterials such as nano-silica, nano-aluminium dioxide, nano-ZnO, and nano-montmorillonite have been increasingly integrated into traditional leather manufacturing systems in recent years to augment the tanning process, which has shown to work efficiently by leveraging their smaller sizes, expanded surface areas, and higher reactivities [24-28]. By optimizing the surface areas and enhancing chemical reactivities, these potential nanomaterials can successfully be applied in leather manufacturing which may result in the production of higher-quality leather materials [29-31]. Surface-modified nanoparticles work as crosslinking agents which enhance the stability of tanned leathers by making robust networks between tanning chemicals and collagen molecules. Among different nanomaterials, graphene oxide (GO) stands out as an excellent choice for use in raw leather processing as a potential nano-tanning agent because of its distinctive sheet-like structures which facilitate the formation of nanosheets with diverse functional groups. GO can be dispersed in aqueous solutions and allows the formation of crosslinking networks in leathers through chemical bonding with the influence of nano-effects [27].

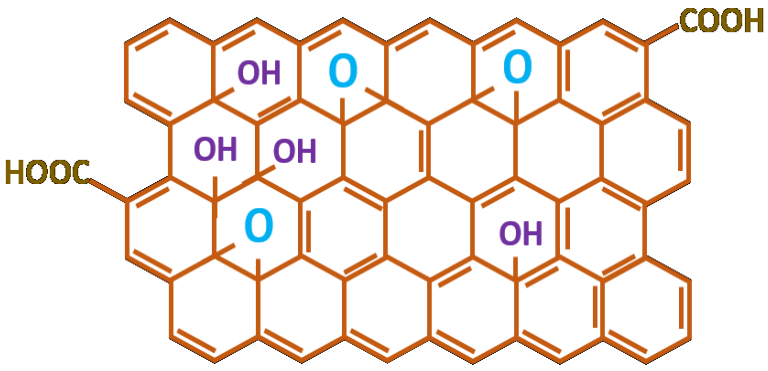

Figure 1. Structure of Graphene Oxide (GO)

On the other hand, due to higher surface area and stability, TiO_2-based nanocomposite has attracted considerable attention for its diversified applications. Furthermore, surface-modified nanoparticles with smaller diameters may function as crosslinking hotspots which can successfully facilitate the

formation of stable cross-linking networks [32]. The aim of the current study was to address and minimize the issue of chromium pollution stemming from various leather industries by developing an eco-friendly tanning agent using nanotechnology. The study initially concentrated on the synthesis and characterization of new PEG-TiO_2-GO nanocomposites from PEG-modified TiO_2 particles combined with GO nanosheets. Then, the present study focused on the potential applications of new nanomaterials in leather tanning processes as well as the evaluation of resulting leathers by conducting different physico-mechanical tests. The novel and innovative approach replaces the applications of toxic chromium compounds by GO-based nanocomposite in raw leather tanning processes to control the environmental pollution load caused by various tannery industries.

It also offers an improvement in the compatibility of leathers with polymer matrices. To reduce environmental pollution arising from leather manufacturing systems, GO-based nanocomposites were introduced in tanning and physical tests of tanned leather were performed. The present study also concentrated on the reduction of tannery wastewater pollution and determined different environmental parameters such as total dissolved solids (TDS), total suspended solids (TSS), chemical oxygen demand (COD), and biochemical oxygen demand (BOD) in the tanning effluents obtained from the applications of both the traditional chrome tanning agent and the new nano-tanning agent.

EXPERIMENTAL

Materials and Methods

Analytical-grade chemicals and reagents were employed for the synthesis and analyses of synthesized nanocomposite materials while commercial/industrial-grade chemicals and reagents were used in the processing of raw leather samples. Graphite fine powder (98% extra pure), sodium nitrate ($NaNO_3$), potassium permanganate ($KMnO_4$) purified, sulfuric acid (H_2SO_4) (98% v/v), hydrogen peroxide (H_2O_2) (30% v/v), hydrochloric acid (HCl) (37% v/v), titanium dioxide (TiO_2) (extra pure), and polyethene glycol 6000 were purchased from the Sigma Aldrich, USA and used without any further purification. Potassium dichromate ($K_2Cr_2O_7$), mercury sulfate ($HgSO_4$), ferrous ammonium sulfate, ferroin indicator, sodium hydroxide (NaOH), sulfuric acid (H_2SO_4), silver sulfate (Ag_2SO_4) was purchased from Thermo-Fisher Scientific, India. All reagents were prepared using distilled water, and the solutions and glassware were autoclaved before their use. Goat skins were collected from the leather processing workshop at the Institute of Leather Engineering and Technology (ILET), University of Dhaka, Bangladesh. Figure 1 shows outlines the multistep preparation of graphene oxide-based nanocomposites and their corresponding applications in leather processing.

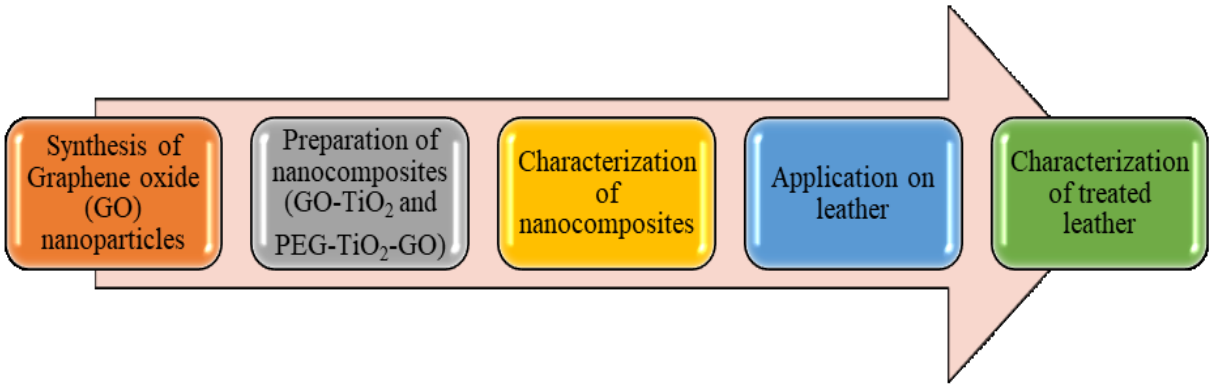

Figure 2. Schematic representation of synthesis of nanocomposites and their applications in raw leather processing

Synthesis of Graphene Oxide (GO) and GO-TiO_2 nanocomposite

The synthetic process of graphite oxide (GO) from graphite fine powder has been reported previously in literature which is generally known as a "modified Hummers method" [33]. To synthesize GO, 120 mL of conc. sulfuric acid solution was placed in a beaker. 3 g of $NaNO_3$ was slowly added to the acid with continuous stirring at a temperature below 5 °C for 30 minutes. Subsequently, 3 g of graphite powder was added, and the mixture was stirred for 2 h at 5 °C after that, 12 g of $KMnO_4$ was gradually added while maintaining a low temperature (<5 °C) for 1 h. The resulting mixture was then stirred for 12 h at room temperature. To prevent overheating, 300 mL of distilled water was slowly added and the mixture was stirred at 98 °C until it changed colour from black to brown. After cooling, 20 mL of 30% H_2O_2 solution was added slowly to the resulting mixture to complete the reaction with $KMnO_4$. The resulting solution was filtered and washed repeatedly with distilled and deionized water until it showed a pH of 6. Finally, the GO product was separated and dried in an oven for 24 h.

Graphene oxide (GO) is an excellent choice among other materials to use as a nano-tanning agent due to its characteristics and structural feature which is comprised of nano-structured sheets with hydrophilic functional groups that facilitate their dispersion in water to form cross-linked networks in collagen fibres. TiO_2 is a non-toxic material which can be used as a tanning chemical and it reacts effectively with leather's collagen carboxyl groups. To enhance tanning effects, TiO_2 was combined with GO using a hydrothermal process. During the synthesis of GO-TiO_2 nanocomposite, 1.0 g of synthesized graphene oxide (GO) was added to 100 mL of deionized (DI) water in a beaker and the mixture was stirred for 1 h. In a separate beaker, 2.0 g of Titanium dioxide (TiO_2) was dissolved in 10 mL of DI water and the mixture was stirred for 1 h as well. Both solutions were then subjected to sonication for about 2 h. Subsequently, the two solutions were combined and then stirred for an additional 2 h. The resulting mixture was further sonicated for 6 h and then stirred for 2 h at a temperature of 45 °C. The mixture was autoclaved at 180 °C for 2 h. The mixture was then cooled to room temperature, filtered, and washed with distilled water which successfully yielded the GO-TiO_2

nanocomposite. Finally, the composite was dried in an oven for 24 h. The schematic diagram of the preparation of GO-TiO_2 nanocomposite has been summarized in Figure 3.

Figure 3. Synthesis of GO-TiO_2 nanocomposite

Hydrothermal process was used to synthesize GO-TiO_2 nanocomposites and the reaction scheme for the synthetic process has been displayed in Figure 4.

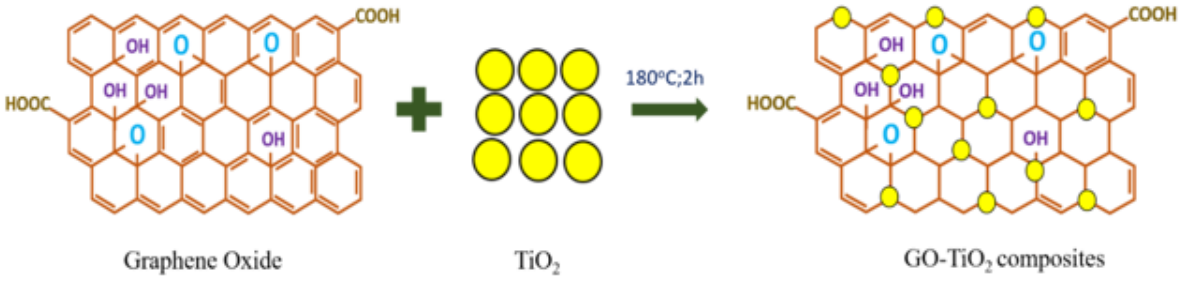

Figure 4. TiO_2-GO nanocomposite synthesis

Synthesis of GO-TiO_2-PEG (GTP) nanocomposite

Polyethylene glycol was used to modify the surfaces of TiO_2 nanoparticles. PEG-loaded Titanium-di-oxide particles (PEG-TiO_2) were incorporated into graphene oxide nanosheets to make GO-TiO_2-PEG nanocomposite which later was applied in the leather tanning process. To prepare the GO-TiO_2-PEG nanocomposite, 1.0 g of synthesized graphene oxide (GO) was mixed into 100 mL of DI water and the mixture was stirred for 1 h followed by 2 h of sonication. In a separate process, 2 g of polyethylene glycol (PEG) was dissolved in 100 mL of DI water at 45 °C temperature. Then, 2 g of TiO_2 was added to the PEG solution and the mixture was stirred for 2 h. This TiO_2-PEG solution was then mixed into the GO solution. The GO-TiO_2-PEG mixture was sonicated for 3 h and then stirred for an additional 2 h at

45 °C. Subsequently, the solution was autoclaved at 180 °C for 2 h, followed by filtration and washing with DI water which yielded the desired composite material with a 1:2:2 ratio of components. As a resulting these steps, the material was oven-dried. The resulting final GO-TiO_2-PEG composite was dried in the oven for 60 h. Figures 5 and 6 show the different synthetic steps for making the GO-TiO_2-PEG nanocomposite material.

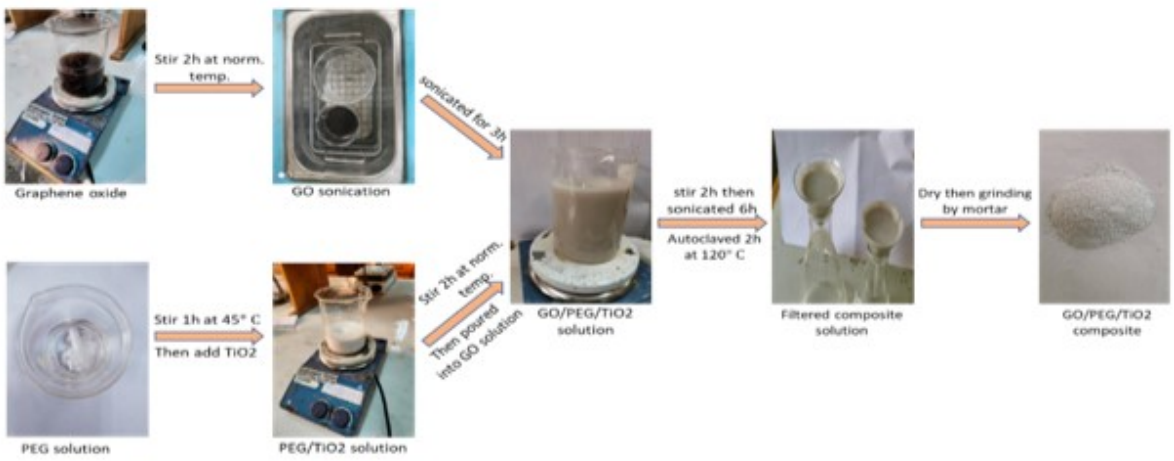

Figure 5. Synthesis of GO-TiO_2-PEG nanocomposite

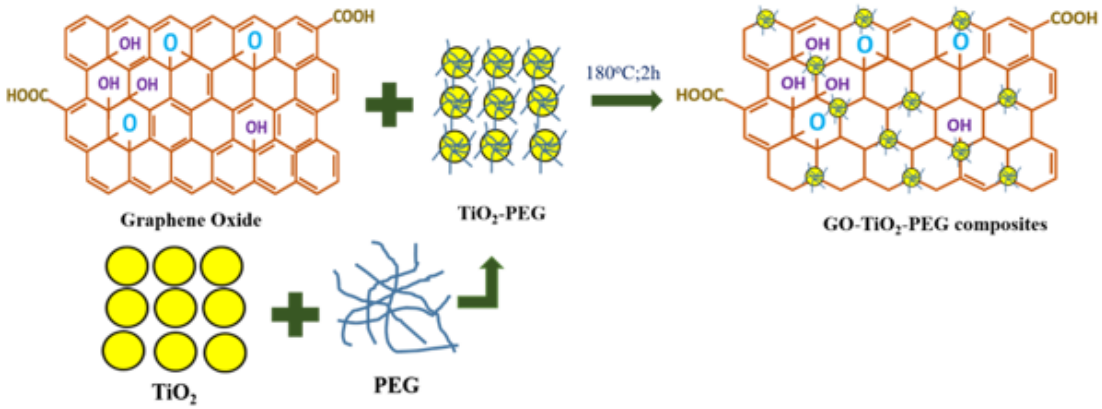

Figure 6. PEG-TiO_2-GO nanocomposite synthesis

Characterization of GO, GO-TiO_2 nanocomposite and GO-TiO_2-PEG nanocomposite

The particle sizes and sizes distributions of Graphene Oxide (GO), GO-TiO_2, and PEG-GO-TiO_2 composites were measured using the Dynamic Light Scattering method (DLS) (Malvern, Zetasizer Waco series) which is also known as Photon Correlation Spectroscopy. Different standard analytical techniques such as FT-IR (model ALFHA II, spectrophotometer (BRUKER, Germany), BRUKER AXS

diffractometer D8 (Germany), TG/DTA 7200 EXSTAR, (Hitachi, Japan) and JSM -6490LA, JEOL (Japan) were employed to analyze the functional groups, crystallinity or undefined (XRD) properties, thermal and morphological characteristics of the synthesized GO, GO-TiO_2, and PEG-GO-TiO_2 materials.

Application of GO, GO-TiO_2 (GT) and GO-TiO_2-PEG (GTP) nanocomposites in leather processing

Four salted goat skin samples were collected from the ILET leather processing lab and the mass of each raw leather sample was measured separately. The leather samples were rinsed thoroughly with fresh water and they were prepared for the beam house operation. The raw leather samples were soaked in a drum which helped reverse the curing process and remove impurities like manure, blood, and dirt. Lime and sodium sulfide mixture was used in the liming process and it took three days to disintegrate hair and wool as well as it also plumped the hides. Adipose tissues were mechanically removed from the flesh side during the fleshing process. A deliming process was carried out to adjust the pH and to remove excess limes. The bating process was accomplished to improve the grain and overall quality of the pelts. A summary of the tanning processes is shown in Table 1.

Table 1. Tanning processes with GO-Nano Composites tanning material

Soaking, liming, bating, and washing procedures were performed conventionally				
	%	Chemicals	Time	pH
Pickling	80	Water		
	7	Salt		
	1	Sodium Formate		
	0.2	Impropel CO	20’	
	0.5	Formic acid (1:10) (20’+20’)	40’	
	1	H_2SO_4 (1:10) (30’+30’+30’)	90’	
	0.5	Hypo	30’	6
Tanning	½ picked bath			
	0.2	Hypo	30’	
	4	RWP (Pre-tanning System)	45’	
	1/3/5	GO-Nano Composites	6’	6
	0.2	Formic acid (1:10)	30’	4.5
	0.2	Bushan		
	0.2	Sodium-bi-carbonate (30’+30’+30’)	90’	
Neutralization and fat liquoring were performed conventionally				

Finally, the pickling process was carried out which lowered the pH to 6 and thus enhanced the absorption of GO-containing tanning substances. A tanning drum was filled up with 80% water and the

de-pickled goat skin. A mixture of NaAc, $NaHCO_3$, and H_2O (1: 1: 10) was used to adjust the pH of the pickle bath at 6. This pH condition was observed to be ideally suitable for the penetration or cross-linking of GO-containing tanning agents with leather fibres [27]. The reaction mixture was rotated for 2 h at pH 6. After that, 10% dilute formic acid solution was added gradually to obtain the optimum pH of 4 in the reaction mixture. 3% GO nano-tanning agent was added, and the resulting mixture was placed in a drum which was spun for 6 h. Figure 7 shows all the processes which have been carried out to make crust leathers by tanning with nanocomposite materials.

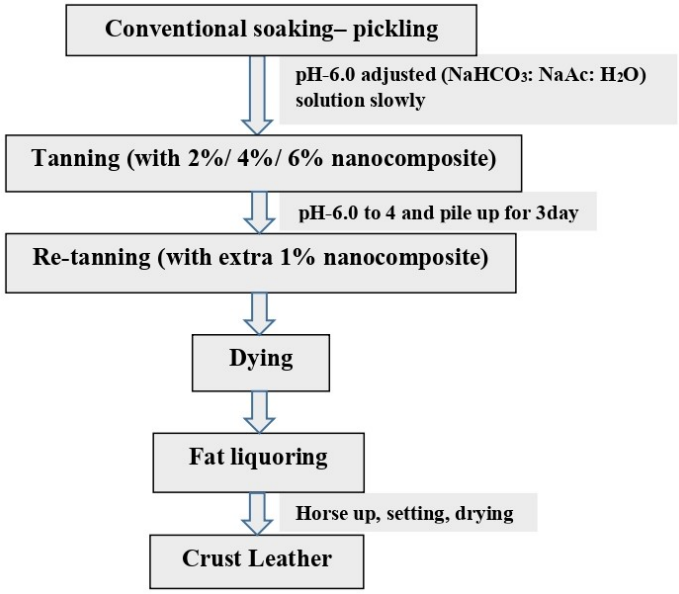

Figure 7. Flowchart of the whole procedure of making nanocomposite-tanned crust leather

After tanning with new nano-tanning agents, specific mechanical procedures were employed to modify the surfaces of leather materials. Machine-operated sammying (using pressurized rollers) was used to eliminate excess moisture content. The splitting and trimming of the resulting leather samples were carried out by using the appropriate machine. Subsequently, the leathers were neutralized, re-tanned using 1% nanocomposite, dyed with appropriate anionic brown dye solutions, and subjected to a fat liquoring with 10.5% mixer of fat (sulphited-3%, anionic 1.5%, synthetic 2%, semisynthetic 2%, and waterproof fat 2%) in process. The resulting leathers were then dried for four days in sunlight, followed by toggling, staking, and ironing in sequential order which eventually yielded the crust leathers (Figure 8).

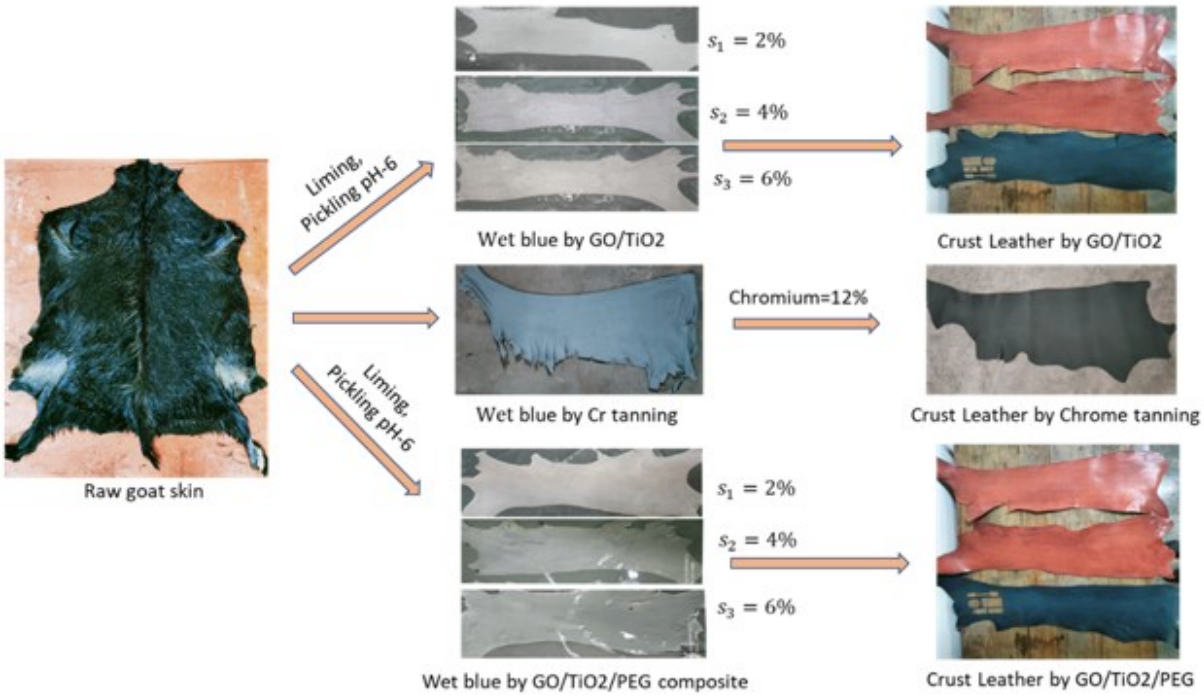

Figure 8. Different sequences in leather tanning process with nanocomposites

Characterization of leather samples

A high-resolution Field-Emission Scanning Electron Microscope (FESEM, Model: JSM -6490LA, JEOL) was used to study the surface morphology of the leather samples tanned with synthesized nanomaterials. The micrograph of the cross-sectional area of leather was captured at x50000 magnification. Fourier-transform infrared (FT-IR) spectroscopy techniques (ATR-FTIR BRUKER, Model ALFHA II, and spectrophotometer) were applied to investigate the presence of different functional groups in the finished leather samples. The FT-IR measurements covered the range of 400 to 4000 cm^{-1}. A Perkin-Elmer TGA 8000 instrument was used to conduct the thermogravimetric analysis (TGA) under a nitrogen environment. The TGA analysis was carried out in the temperature range of 25 to 700 ^{o}C at a heating rate of 10 ^{o}C /min.

Physical and mechanical tests were carried out on the conventional and GO nanocomposite-treated leathers following the procedures of international standard methods. Different physicomechanical properties such as shrinkage temperature, tensile strength, stitch strength, tear strength, flexing endurance, and crack resistance were investigated, and the results were compared to understand whether the applications of nanocomposites in the tanning process yielded the leathers with desirable physical properties which are very similar to those found in the chrome-tanned leathers. The specific international standards adhered to these tests have been listed in Table 1.

Table 2. The standard methods [34-39] of different physical tests which were carried out in the leather samples

S. l. No	Test name	Standard Norm
1.	Shrinkage Temperature	SATRA TM-17: 1997
2.	Tensile strength test	IUP-6
3.	Stitch tear strength test	DIN-53329
4.	Simple tear strength test	SATRA PM-162
5.	Grain crack resistance test	IUP-09
6.	Flexing endurance	SATRA PM-55

The leather samples were cut parallel to the direction of strength to perform the tensile test, stitch tear test, and Baumann tear test. The tensile tester (STD 172, Wright & Sons Ltd. England) was used to carry out the tensile strength test, stitch tear test and Baumann tear test. The physical test results were compared with the acceptable international standard values (Table 3).

Table 3. International standard values physical test of leather [40]

Physical test	Standard value	Physical test	Standard value
Tensile strength	Min. 200 kg/cm^2	Simple tear strength	Min. 30 kg
% of elongation	30-40 %	Grain crack resistance	16 kg
stitch tear strength	80-120 kg/cm	flexing endurance (after 100000)	peppiness scale rating (1-2)

Characterization of residual tanning liquor

The residual liquor generated from the tanning of raw leathers with nanocomposites was collected, and the liquor was analyzed to evaluate its quality. Different standard quality parameters such as total dissolved solids (TDS), total suspended solids (TSS), chemical oxygen demand (COD), and biological oxygen demand (BOD), were measured in the residual liquor and the results were compared with those obtained from the conventional chrome tanning liquor.

Total dissolved solids (TDS)

A systematic procedure was employed to determine the TDS in the liquor samples. 50 mL of homogeneous liquor was transferred into a clean beaker (weighed out previously) while maintaining agitation. Subsequently, the liquor contents were filtered and washed three times. The beaker along with the filtrate was then dried in an oven at 105 ^{o}C until all moisture content was removed. After cooling, the beaker was reweighed, and the TDS was calculated in milligrams per litre (mg/L). This process was repeated three times for each sample and an average result was taken. The following equation was used to calculate TDS concentration.

$$\text{Total dissolved solids (mg/L)} = \frac{(a-b) \times 1000}{50\ mL\ sample} \quad (1)$$

Where,

a = the weight of the dried residue along with the beaker in mg

b = weight of empty beaker in mg

Total suspended solid (TSS)

To measure total suspended solids (TSS), 50 mL of the liquor sample was carefully filtered through filter paper. The residue that remained on the filter paper was subsequently dried in an oven at about 105 °C until a constant weight was obtained. The increase in mass of the filter paper after drying provided the quantity of total suspended solids in the respective sample. This procedure was repeated three times to determine TSS in the other seven samples. The following equation was used to determine TSS in all liquor samples:

$$\text{Total suspended solids (mg/L)} = \frac{(a-b) \times 1000}{50\ mL\ sample} \quad (2)$$

Here,

a = mass of dried filter paper after filtration in mg

b = mass of empty dried filter paper in mg

Chemical oxygen demand (COD)

In the COD measurement procedure, 20 mL of a blank solution and 20 mL of the respective sample were mixed into a reaction flask. Boiling aids and 10 mL of a mercury-containing $K_2Cr_2O_7$ solution were added to the flask. Subsequently, 30 mL of Ag_2SO_4 solution with H_2SO_4 was carefully introduced into the flask while it was being cooled in ice to avoid overheating. A reflux condenser was attached to the reaction flask and the reaction mixture was heated at 150 ^oC for 1.5 h. The resulting mixture was cooled to room temperature and diluted to 100 mL with the addition of distilled and deionized water. Two to three drops of ferroin indicator solution were added. Finally, the unreacted $K_2Cr_2O_7$ was estimated by titrating with $(NH_4)_2Fe(SO_4)_2{\cdot}6H_2O$ solution until the colour changes occurred from blue-green to red-brown. The chemical oxygen demand of the sample has been calculated using the following equation.

https://doi.org/10.31881/TLR.2024.036

$$\text{COD (mg/L)} = \frac{(V_b - V_s)\ X\ C\ X\ f\ X\ D_s}{V_e} \quad (3)$$

Here,

V_b = Volume of the $(NH_4)_2Fe(SO_4)_2 \cdot 6H_2O$ solution in mL consumed in the blank.

V_s= Volume of the $(NH_4)_2Fe(SO_4)_2 \cdot 6H_2O$ solution in mL consumed during the sample titration.

V_e= Volume of the sample (20 mL)

C= Concentration of the $(NH_4)_2Fe(SO_4)_2 \cdot 6H_2O$ solution in mol/L (C= 0.12 mol/L)

f = Equivalent factor (f= 8000 mg/mol)

D_s= Dilution factor (the time of dilution= 100 times).

Biological oxygen demand (BOD)

The following procedure was used to measure BOD in the liquor samples obtained from the leather tanning process. 43.5 mL of the sample was transferred to a BOD bottle. A magnetic stirring rod was placed in the sample bottle, and a rubber quiver was inserted into the bottle's neck in which two sodium hydroxide pellets were delicately placed with tweezers to ensure that they mixed up with the wastewater sample. After that, the sample bottle was tightly screwed onto the OxiTop. The temperature of the Oxitop-covered measuring vial was maintained at 20 ^oC for five days in an incubator. When the measurement temperature is reached (within 1 to 3 h through the Auto Temperature Indicator), the Oxitop automatically commences the measuring of oxygen consumption while continuously agitating the liquid sample for the entire five days. The measured value (digits) which was being displayed in the instrument has been converted into the BOD value by using the following equation:

$$\text{Digits} \times \text{Factor} = BOD_5 \text{ in mg/L} \quad (4)$$

where digits represent the highest reading among 5 days and the magnitude of a factor was considered as 50 (for 43.5 mL sample factor = 50)

The magnitudes of TDS, TSS, COD and BOD measured in all the liquor samples were compared with the standard permissible values of the Department of Environment (DoE), Bangladesh [38]. The results of TDS, TSS, COD and BOD analyses as well as their comparisons with the standard permissible values have been presented in Table 4.

Table 4. Standard permissible values of TDS, TSS, COD, and BOD reported by DoE [41]

Parameter	Standard value	Parameter	Standard value
TDS	2100 mg/L	COD	200 (inland surface) - 400 (irrigated land)
TSS	150 – 500 mg/L	BOD	50 (inland surface) - 250 (irrigated land)

RESULTS AND DISCUSSION

Characterization of Graphene oxide (GO), GO-TiO_2 and GO-PEG-TiO_2

FT-IR analysis of graphene oxide (GO), GO-TiO_2 and GO-PEG-TiO_2

FT-IR study on the synthesized composites provided significant information on the presence of different functional groups in the respective materials. Figure 9 depicts the presence of various functional groups within the structures of GO, GT, and GTP composites. The FT-IR spectrum obtained from the GO layer reveals the presence of various functional groups such as carboxyl (-COOH), epoxy (C-O-C), hydroxyl (O-H), and carbonyl (C=O) groups in the composite (Figure 9A). The intense resonance that appeared at 3411 cm^{-1} might be attributed to the carboxyl groups (O-H) formed by the integration of water molecules. The ketone group (C=O) within the structures of composites provided significant resonance at 1726 cm^{-1}, whereas the main graphitic component's (C=C) showed resonance at 1627 cm^{-1} indicating the occurrence of sp^2 hybridization [42]. Similarly, the IR-resonances at 1387 cm^{-1}, 1084 cm^{-1} and 731 cm^{-1} respectively might probably have originated from the stretching vibration of epoxy groups along their C-O-C axes, C-O stretching of alkoxy groups and C-H bending vibrations [43] (Figure 9A). The characteristic resonances at 3201 and 1620 cm^{-1} in Figure 9B might have appeared due to the stretching vibration of the hydroxyl (–OH) group and the C=C skeletal vibration from the structural moieties of graphene oxide (GO). Additional IR resonances observed at 1720, 1400, and 1055 cm^{-1} might be attributed to the stretching vibrations of carboxylate C=O, carboxyl C–O–C, and alkoxy C–O respectively present in the nanocomposite. The appearance of a broad IR band at 723 cm^{-1} might be related to the stretching vibrations of Ti–O–C and Ti–O–Ti bonds [44]. A significant reduction in the intensities of IR resonances associated with oxygen-containing functional groups in GT spectra in comparison to those observed in graphene oxide suggests a substantial decrease in GO content during the nanocomposites synthesis process which affirms the efficiency of hydrothermal treatment in producing GT nanomaterials.

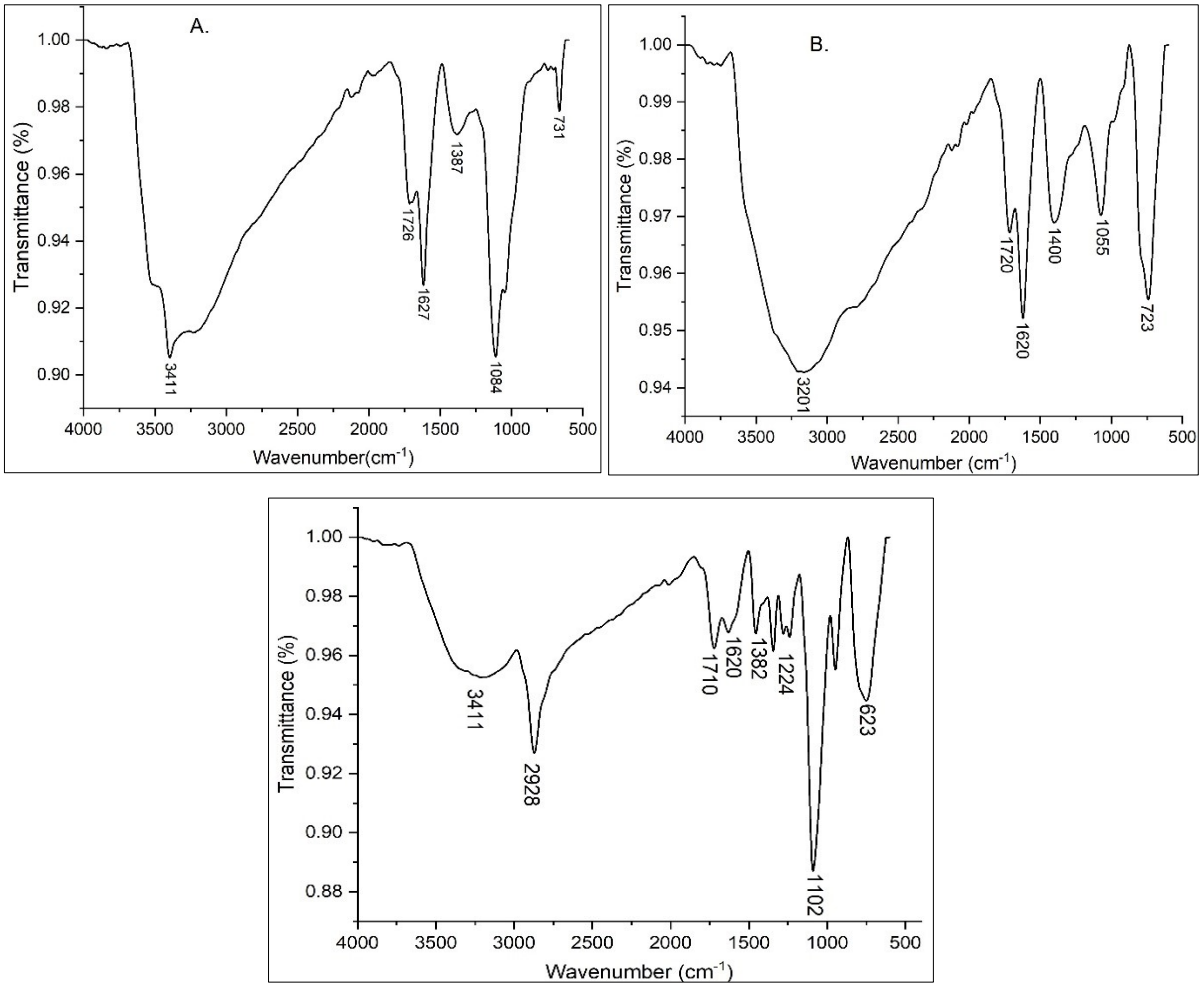

Figure 9. FT-IR spectra of A. GO; B. GO-TiO_2 & C. GO-TiO_2-PEG composite

Figure 9(C) shows broad resonances at 3411 cm^{-1} and 1710 cm^{-1} respectively which might have originated due to the stretching vibrations of O-H and C=O groups from carbonyl and carboxyl groups present in graphene oxide. The IR band observed at 1382 cm^{-1} might be attributed to C-O-C, and the peak at 1620 cm^{-1} could be related to the C=C functional moiety available in the respective composite [45]. The presence of PEG in the nanocomposites caused the appearances of sharp resonances at 2928, 1710, and 1102 cm^{-1} in the spectra which might have been associated with the stretching vibrations of C-H, C=O, and C-O functional moieties respectively. Additionally, O-H bending vibrations from PEG might cause the appearance of IR resonance at around 1224 cm^{-1} (Figure 9C) [46]. The characteristic peak appeared at 623 cm^{-1} indicating the presence of Ti-O-Ti and Ti-O-C bond patterns in TiO_2. The characteristics of FT-IR resonances observed in the spectra of GO and GO-TiO_2-PEG composites were found to be very similar which evidenced the incorporation and dominance of graphene oxide within the surfaces of both GO-TiO_2 and GO-PEG-TiO_2 composites materials.

DLS analysis for particle size distribution

The sizes and shapes of particles as well as their distributions within the synthesized GO, GO-TiO_2, and GO-TiO_2-PEG composites materials were determined by using the Dynamic Light Scattering (DLS) technique [47]. The results of DLS analysis on the graphene oxide (GO), GO-TiO_2, and GO-TiO_2-PEG composites have been illustrated in Figure 10. The average particle sizes of GO, GT, and GTP were found as 369 nm, 390 nm, and 432 nm respectively. A single sharp peak was evident in each case, with polydispersity indices of 23%, 30%, and 29% respectively. The overall efficiency and penetration capability are contingent upon the particle size distributions where the smaller particle diameters are observed to be associated with better performances [48]. The particles with smaller sizes work more efficiently as nano-species and they exhibit better nano-effects in the leather tanning process.

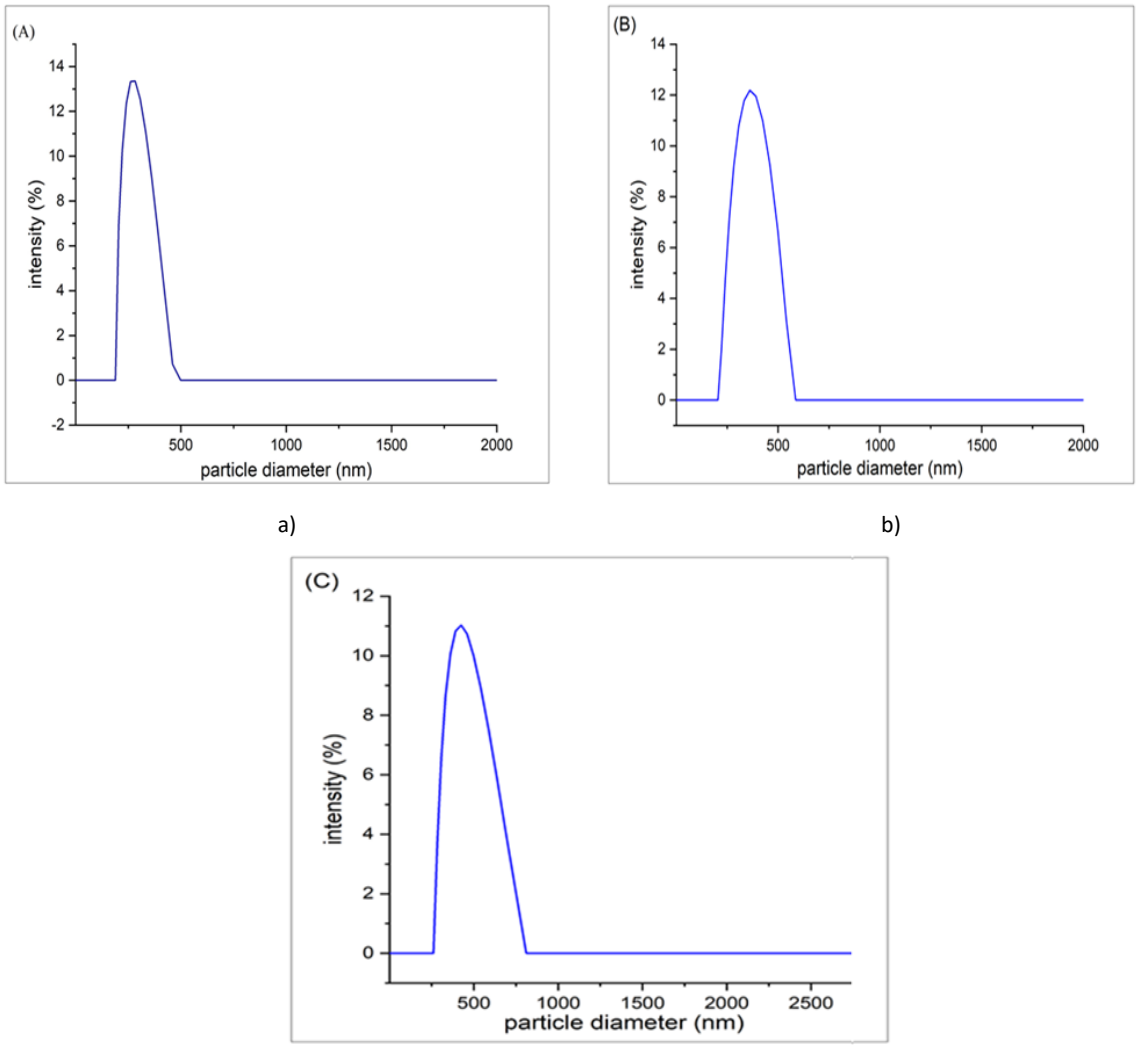

a) b)

c)

Figure 10. Particle size distributions in a) GO; b) GO-TiO_2; c) GO-TiO_2-PEG composite

XRD analysis of Graphene Oxide (GO), GO-TiO_2 (GT) *and GO-PEG-TiO_2 (GPT)*

An X-ray diffraction (XRD) study was conducted to assess the crystalline properties of GO (graphene oxide) particles and the respective nanocomposite materials, GT, and GTP (Figure 11). The hydrophilic GO particles displayed a robust peak at 2θ = 10.2°, suggesting that water molecules have been trapped between the nano-layers and it also demonstrated the crystallinity properties of nanomaterials. Another resonance peak at 42.4° might have indicated the residual MnO_2 species as a byproduct of the GO synthesis reaction with $KMnO_4$. The results of the XRD analysis confirmed the successful formation of GO nanoparticles (Figure 11). In the case of GT nanocomposites, the diffraction pattern was observed to be very close to those obtained from pure TiO_2. The peaks at 2θ values of 25.1°, 37.4 °, 47.6°, 54.4°, 56.2°, 62.9° and 69.9° were indexed as anatase TiO_2 crystal planes [49]. It was noted that the peak at 10.2° which was assumed to appear for the trapped water in GO was absent in the XRD spectra of GT indicating the release of water molecules during the synthesis of nanocomposite. Importantly, the structures of all composites showed the crystal planes of both anatase and rutile phases revealing that the introduction of graphene oxide did not alter the original structural feature of TiO_2. The absence of GO diffraction peaks in GT was attributed to TiO_2 intercalation disrupting GO's regular stacking patterns.

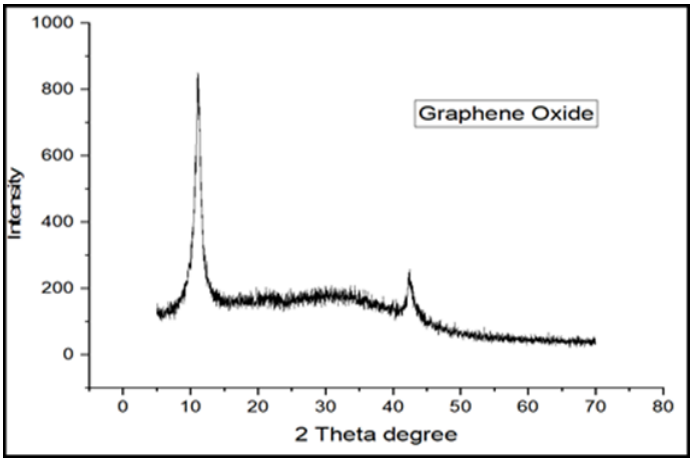

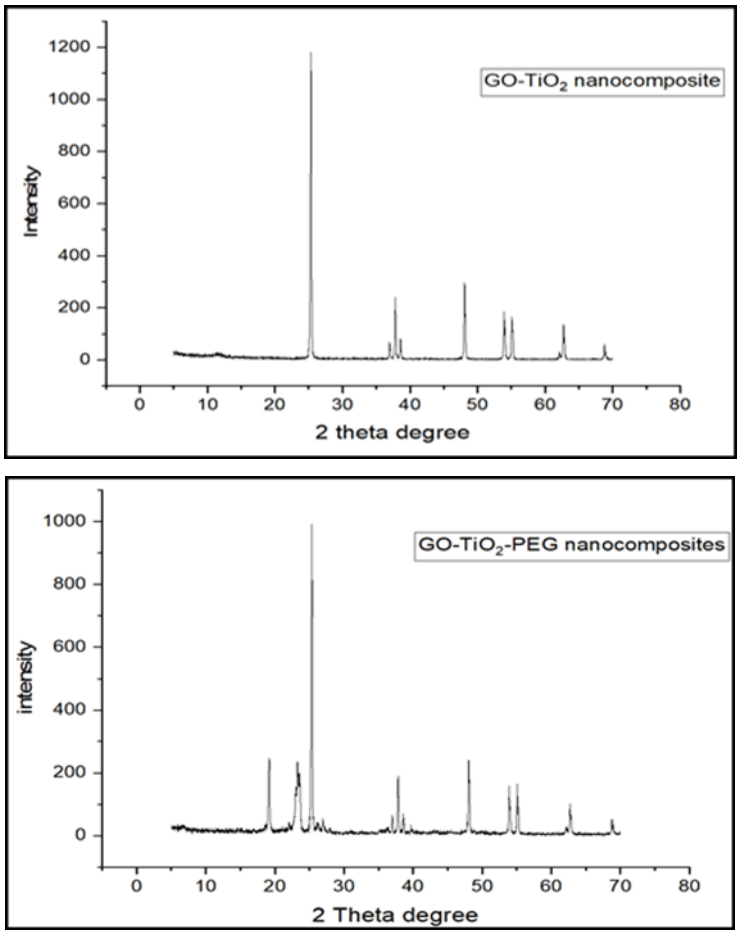

Figure 11. XRD pattern of graphene oxide, GO-TiO_2 and GO-TiO_2-PEG nanocomposites

The results of XRD analysis also indicated the incorporation of PEG and TiO_2 nanoparticles in GTP composites. The peaks that appeared at 19.3° and 23.2° were attributed to PEG structure while the resonances at 25.1°, 37.4°, 47.6°, 54.4°, 56.2°, 62.9° and 69.9° were assigned to TiO_2. There was no peak at 10.2° which affirmed that TiO_2 intercalation might have disrupted GO's stacking in the GTP composites.

SEM study on Graphene Oxide (GO), GO-TiO_2 and GO-PEG-TiO_2

The surface characteristics of GO as well as synthesized GT and GTP composites were analyzed by using the SEM technique and the corresponding results have been depicted in Figure 12. The micrograph of the synthesized GO indicates the successful formation of a single layer of graphene oxide (Figure 12 A). The SEM image of GT nanocomposites reveals that TiO_2 nanoparticles are evenly distributed in spherical shapes, although they show a tendency to aggregate (Figure 12B). The SEM image also shows that the lattice structure in the GT nanocomposites is not visible due to the higher concentration of TiO_2 in comparison to those observed in the GO sheets. However, the SEM image of GTP composites also displays a uniform distribution of TiO_2 nanoparticles with spherical shapes, but they show a

tendency to agglomerate due to the stickiness of PEG (Figure 12C). Similarly, the lattice structure in the GTP composites is not found to be significant because of the presence of higher concentrations of both TiO_2 and PEG in comparison to those present in the GO sheets as indicated in the respective SEM images.

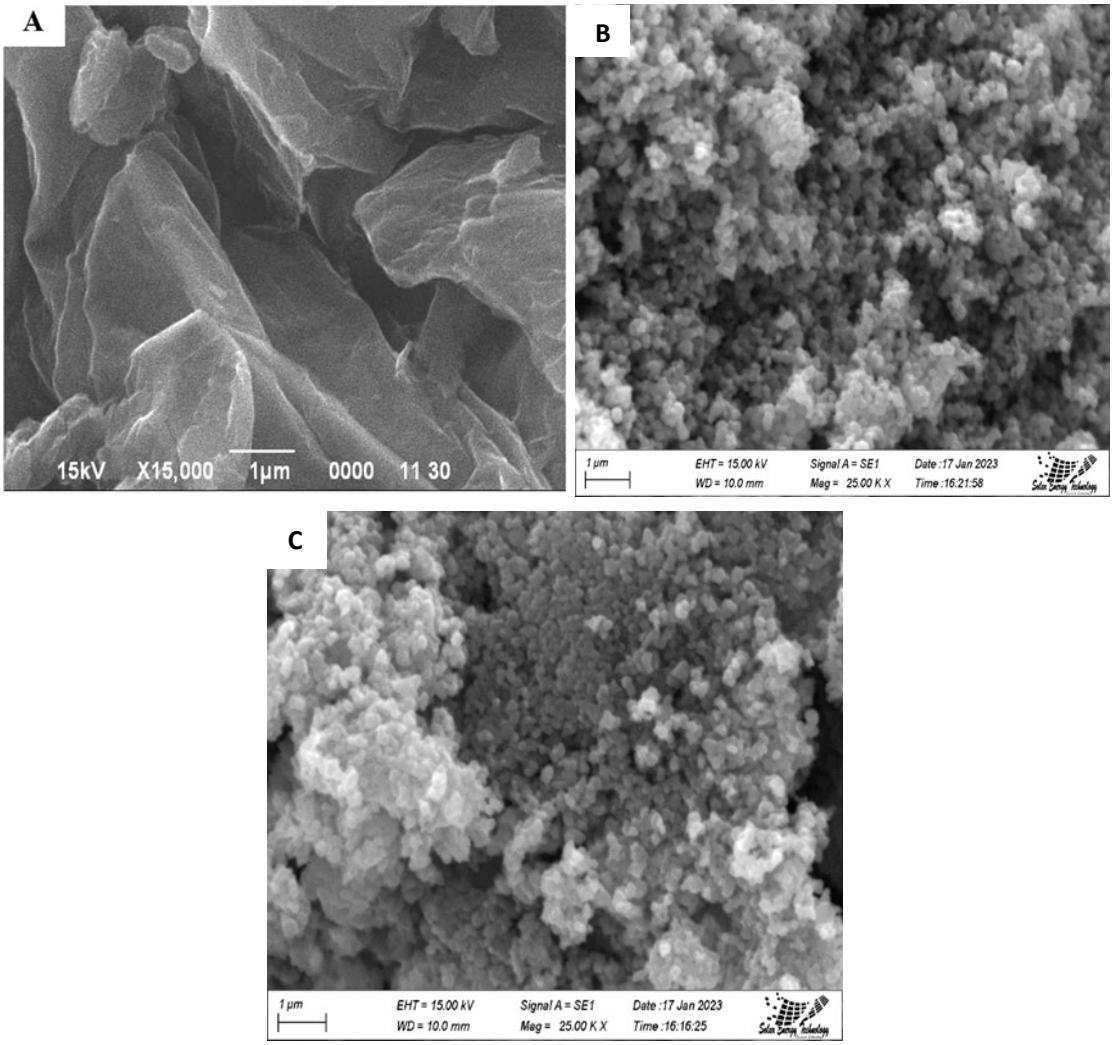

Figure 12. SEM image of: a) GO; b) GO-TiO_2; c) GO-TiO_2-PEG nanocomposites

Characterization of leathers manufactured with graphene oxide-based nanocomposites

Fourier-transform infrared spectrophotometric (FT-IR) study of nanocomposites tanned leathers

The FT-IR analysis on the leathers tanned with nanocomposites provided significant information on different functionalities present in the respective samples. ATR-FTIR spectra were recorded within the range of 4000 and 500 cm^{-1}. Sharp IR resonances were observed between 3600 to 3400 cm^{-1} in the FTIR spectra indicating the presence of the hydroxyl group in the respective leather samples which

were tanned with nanocomposite materials. The appearances of IR bands between 1850 to 1080 cm^{-1} revealed significant detailed information on functional moieties present within the structures of leathers tanned with the synthesized nanocomposite materials (Figure 13).

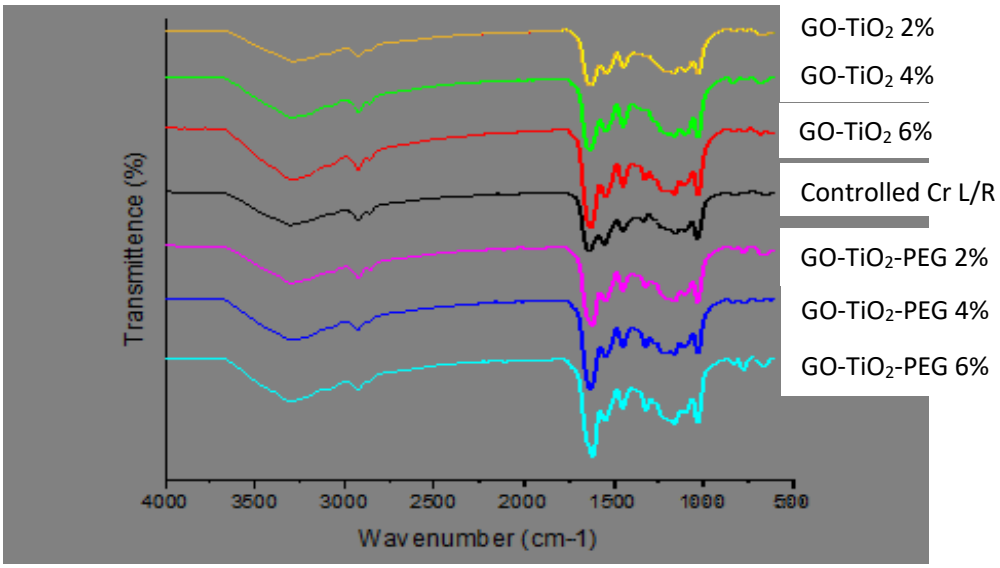

Figure 13. ATR-FTIR spectra of nanocomposites tanned leather

FT-IR spectra of the leathers tanned with GT and GTP nanocomposites showed characteristic resonances for different functional groups which were very similar to those observed in the spectra of chrome-tanned leathers. There were no significant differences observed among the resonances that appeared in the FT-IR spectra of chrome-tanned leather and nanocomposite-tanned leather samples which revealed that the application of new tanning nanocomposite materials yielded the leathers which were characteristically the same as those obtained by chrome tanning method. This also suggested that leathers processed with nanocomposites possessed identical structural features as observed in conventional chrome-tanned leathers and nanocomposites might have bonded with collagen fibers with different functional groups. The sharp IR resonance at 730 cm^{-1} was highly notable in the spectra of the nanocomposites-tanned leathers which was found as insignificant in the respective spectra of conventionally chrome-tanned leathers suggesting the existence of Ti-O-C and Ti-O-Ti bonding between collagen and TiO_2 particles [44].

Thermal analysis of nanocomposite-tanned leathers

All leather samples were subjected to thermal analysis and this process was carried out using a TGA 8000 TM instrument (Perkin Elmer, USA). During the thermal study, 4 to 5 mg of each finished leather sample was heated at 700 °C in a platinum pan at a constant rate of 10 °C per minute under the constant flow of N_2. Figure 14 shows the loss in mass of tanned leather upon heating. With the changes

in temperatures from 30 to 600 °C, all leather samples showed similar weight losses suggesting the occurrences of two distinct degradation processes. The initial reduction in masses was observed at a temperature range of 90 to 120 °C which might be attributed to the evaporation of both free and bound water contained within the samples. The major degradation in masses of leather samples was observed between 230 and 600 °C which indicated the breakdown of collagen fibers. Interestingly, the thermal characteristics of the leathers processed in dry conditions differed from those obtained in wet conditions. The major weight loss (50–60%) was observed in all processed leather samples at 300 to 400 °C as revealed from the TGA graphs which showed sharp breakpoints (shoulder peak) suggesting that the leather species were broken down at that temperature (Figure 14). The results of the TGA analysis of all processed goat leathers were highly comparable to those observed in other similar leather species as reported previously in literature which demonstrated that the leathers decomposed at temperatures between 300 and 400 °C [50,51].

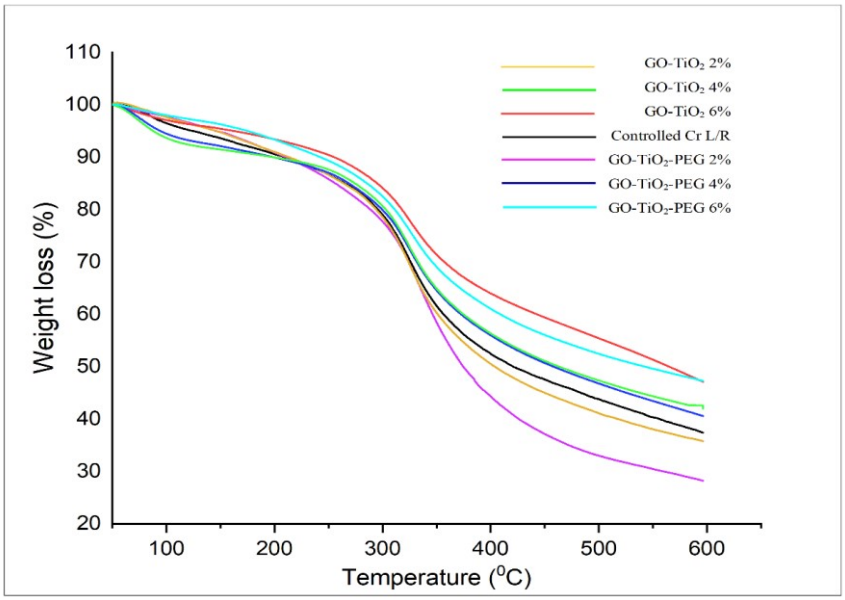

Figure 14. TG analysis of leathers tanned with nanocomposites

Each of the finished goat leathers was found to be stable up to 300 °C as revealed from the TGA data (Figure 14) which indicated their excellent thermal stability. Interestingly, the leathers tanned with GT (6%) and GTP (6%) showed relatively higher thermal stabilities than all other finished leather samples (Figure 14).

FE-SEM analysis of leather tanned with nanocomposite materials

FE-SEM study was carried out to investigate the surface morphology of conventional chrome-tanned leather, GO-TiO_2-tanned leather, and GO-TiO_2-PEG composite-tanned leather. The results of FE-SEM analysis provided significant information on the incorporation of nanoparticles into leather surfaces as well as fibre dispersibility in the respective samples as shown in Figure 15.

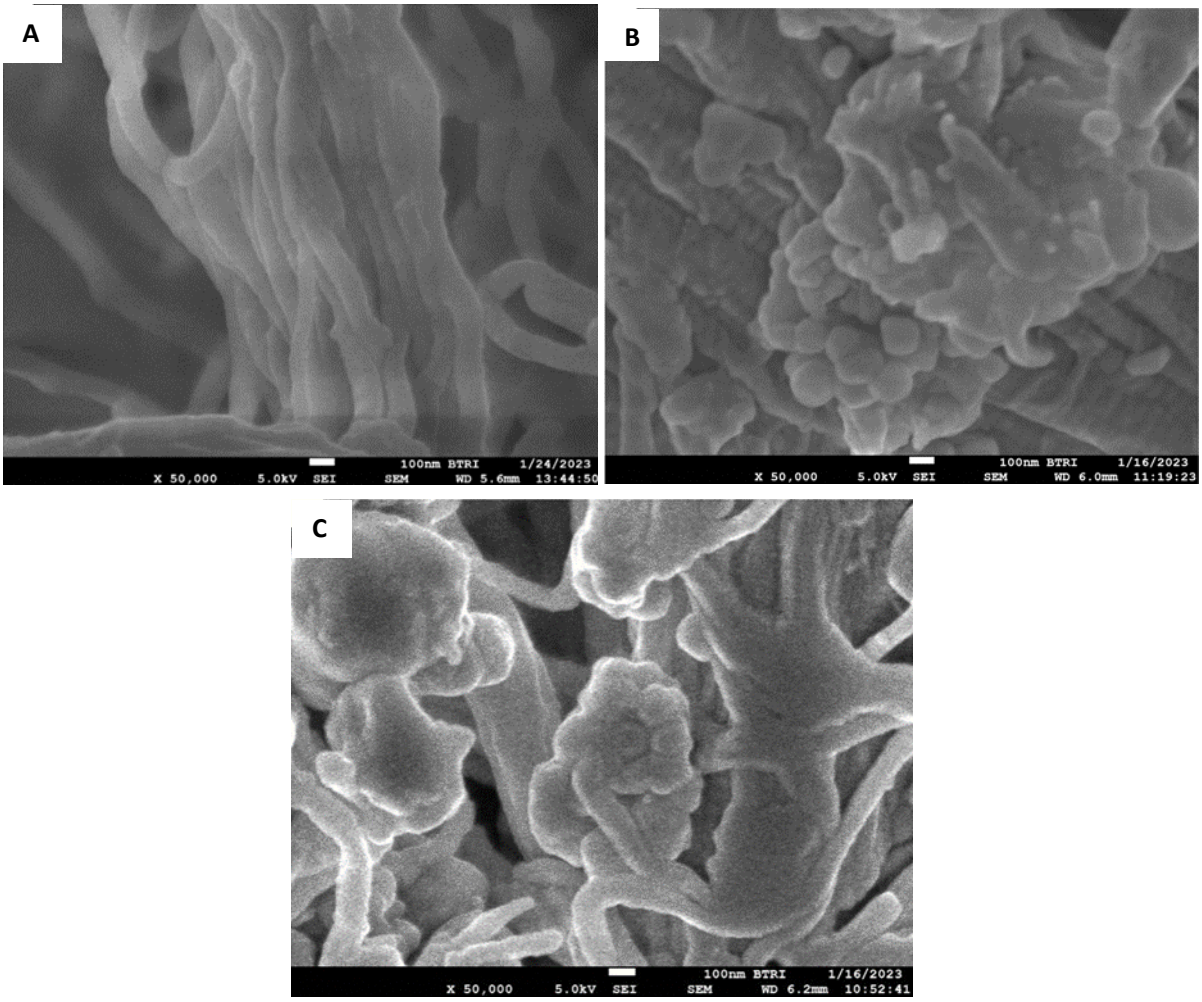

Figure 15. FE-SEM image of a) conventional, b) GO-TiO_2 and c) GO-TiO_2-PEG composite tanned leather

Leathers tanned with chrome-based chemicals exhibit thicker collagen fibres with no apparent visible particles on the surfaces (Figure 15A). In contrast, when GT composites were used in the tanning process, these composites were permeated into the leather surfaces and integrated within the fibres as shown in Figure 15(B). These leather fibres were observed to be well-dispersed, and the nanocomposites formed bonds with the collagen fibres (Figure 15B). Similarly, GTP composites were also permeated into leather surfaces and incorporated into the fibres (Figure 15C). It has been apparent that a larger number of GTP nanocomposites penetrated the leathers in comparison to the

incorporation of GT nanocomposites into the respective leather samples. Furthermore, the leather fibres, in this case, were also observed to be well-dispersed with the bond formation between PEG-GO-TiO_2 nanocomposites and the collagen fibres.

Evaluation of physical and mechanical characteristics of nanocomposite tanned leathers

The leather samples tanned with nanocomposites were subjected to tensile strength test, stitch tear test, Baumann tear, strength test, cracking resistance test, and flexing endurance test. The results of all physico-mechanical tests were compared with the properties of conventional chrome-tanned leathers to evaluate the strengths of leathers processed with nanocomposite materials for their applications in the respective fields. The findings of different physical and mechanical properties of leathers tanned with nano-composites as well as conventional chrome-tanned leather have been displayed in Table 5.

Table 5. Physical and mechanical properties of leathers tanned with nanocomposites and in conventional tanned leathers

Parameters		Chrome Tanned Leather	GO-TiO_2 nano-composite tanned leather			GO-TiO_2–PEG nano-composite tanned leather		
		Controlled	2%	4%	6%	2%	4%	6%
Shrinkage Temperature (°C)		105	90	95	95	90	95	100
Tensile Strength	Horizontal	223	202	213	228	196	209	233
(kg/cm^2)	Vertical	183	147	169	188	133	152	201
Stitch Tear	Horizontal	107	80	87	101	94	102	122
Strength (kg/cm)	Vertical	87	66	71	80	81	90	98
Simple Tear	Horizontal	41	37	42	44	37	40	42
Strength (kg/cm)	Vertical	30	29	30	33	28	31	33
% of elongation	Horizontal	35.5	25.7	26.1	32.3	28.3	23.4	33.7
	Vertical	41.8	32.3	34.2	38.9	38.3	33.6	43.8
Flexing Endurance*		3	3/4	3/4	3	3/4	3	3
Grain crack strength (kg/cm)		38	21	27	33	25	34	30
Distension length (cm)		11.2	7.6	9.5	7.5	8.0	10.1	8.9

*Break peppiness scale rating after 100,000 cycles

The shrinkage temperature of 2% nanocomposite-tanned leather was observed to be slightly lower than that of chrome-tanned leather but higher than that of vegetable-tanned leather (Table 5). The leather samples tanned with 6% GTP nanocomposite exhibited the highest shrinkage temperature which was very close to those observed in the chrome-tanned leathers. In the case of tensile strength and percentage of elongation, nanocomposite-tanned leathers displayed very similar performances to chrome-tanned leathers. Interestingly, the strengths of leathers tanned with GT (6%) and GTP (6%)

nanocomposites exceeded the performances of chrome-tanned leathers as evidenced by the results of various physiomechanical tests (Table 5). Additionally, the elastic properties of nanocomposite-tanned leathers were increased gradually with the application of higher percentages of nanocomposites in the tanning process. The percentage of elongation was observed to be higher in the leathers tanned with 6% of GT and GTP nanocomposites (Table 5). The magnitudes of stitch tear strengths of all nanocomposite-tanned leathers were very close to the international standard value except for the leathers in the vertical position which were processed with 2% and 4% GT nanocomposites respectively. The highest stitch tear strength was observed in the leathers tanned with 6% of both GT and GTP nanocomposite materials (Table 5).

The magnitudes of simple tear strengths measured in nanocomposite-tanned leathers were very similar to the international standard permissible value except for the leathers in the vertical portion which were processed with 2% of GT and GTP nanocomposites respectively. Among all processed leathers, the leathers processed with 6% of GT and GTP nanomaterials exhibited the highest simple tear strengths in comparison to all other processed leather samples. In terms of upper leather criteria, the break peppiness scale rating should fall within the magnitudes of 1 to 3/4 after 100,000 cycles. The nanocomposite-tanned leathers met these criteria and showed this standard value in the respective tests. The results of the Grain crack resistance test for nanocomposite-tanned leather were very similar to those observed in conventional chrome-tanned leather (Table 5). All leathers tanned with nanocomposite materials showed a degree of grain crack resistance which exceeded the international standard values where the application of 6% of GT and GTP nanocomposite in the tanning process yielded the leathers with the highest magnitude of the respective grain crack resistance. The distension of each nanocomposite-tanned leather was observed to be very similar to that of controlled chrome-tanned leather, and all processed leather samples showed results which were very close to the international standard values. Different organic functional groups such as hydroxyl, carboxylic acid, ether etc. might have remained in GO-nanocomposite as well as in the leather fibers. Various interactive forces such as hydrogen bond, covalent bond, dipole-dipole interaction, van der Waals force etc. might have occurred between the structural moieties of GO-nanocomposite and collagen fibers which enhanced the physico-mechanical properties of experimental tanned leathers.

Physicochemical characteristics of residual liquor obtained from the leather tanning process

Different physiochemical parameters such as TDS, TSS, COD and BOD were measured in the residual liquors obtained from the nanocomposites leather tanning process as well as the conventional chrome tanning method where 12% basic chromium sulphate [$Cr(OH)SO_4$] was employed and the results were compared with the respective standard permissible values as reported by Department of Environment (DoE) (Table 6).

Table 6. The magnitudes of TDS, TSS, COD and BOD in nanocomposites-tanned liquor as well as in chrome-tanned liquor

Parameters	Chrome Tanned Liquor	GO-TiO_2 nanocomposite tanned residual liquor				GO-TiO_2 –PEG nanocomposite tanned residual liquor			
	Controlled 12% $Cr(OH)SO_4$	2%	4%	6%	Maximum reduction	2%	4%	6%	Maximum reduction
TDS (mg/L)	183.8	18.3	22.5	34.5	90%	27.3	39.4	47.5	85%
TSS (mg/L)	23.8	2.2	4.9	7.4	91%	2.7	5.1	7.6	89%
COD (mg/L)	4800	1440	1920	2400	70%	1920	2400	2880	60%
BOD (mg/L)	200	50	50	100	75%	50	100	100	75%

The United States Environmental Protection Agency (EPA) recommends the TDS treatment when TDS concentration in waterbody exceeds 500 mg/L. The Department of Environment (DoE) in Bangladesh allows TDS contents in industrial wastewater bodies as 2100 mg/L [41]. The TDS level obtained in residual liquor from the nanocomposite tanning process was much lower than the recommended permissible value of EPA. When the TSS level exceeds 40 mg/L, it can cause cloudiness. DoE permits TSS levels ranging from 150 to 500 mg/L. However, the TSS contents in the residual liquor generated from nanocomposite tanning were found to be below 10 mg/L, which was significantly lower than the tolerable levels reported by EPA and DoE suggesting that wastewater released from the leather tanning process with nanocomposites is safe for aquatic life. In the case of Chemical Oxygen Demand (COD), the EPA recommends an acceptable level of 250 ppm for aquatic life. DoE has established a standard permissible value of COD at 200 mg/L for inland surface water and 400 mg/L for irrigation water. Higher COD levels can be detrimental to aquatic life. The magnitudes of COD measured in the residual liquors obtained from nanocomposite-leather tanning processes were much higher than the threshold values of EPA and DoE (Table 5). A highly significant amount of COD (70%) and BOD (75%) of the effluents decreased from the conventional tanning process when only 2% of GO-TiO_2 nanocomposite was utilized in the experimental group. Almost similar results were found in the case of 2% GO-TiO_2-PEG nanocomposite. The COD and BOD values of the effluents again increase with the increase of the addition of GO-TiO_2-based nanocomposites in leather manufacturing. These results prove that a 2% GO-TiO_2-based nanocomposite tanning agent could be optimized for chemical bonding with the active sites of leather fibres and additional dose does not chemically bond with the fibre. Therefore, the physicochemical parameters of the effluents increase gradually (Table 6). The tolerable limit of Biochemical Oxygen Demand (BOD) is 250 mg/L for irrigation water (for public sewerage systems connected to second-stage treatment) and 50 mg/L for inland water as reported by DoE. The extent of BOD determined in the nanocomposites-tanned liquors was found to be within the acceptable level of DoE (Table 5). However, the magnitudes of BOD were significantly lower than those observed in the chrome-tanned liquors indicating the benefits of the applications of nanocomposites

in raw leather tanning processes as less toxic wastewater is being released from the respective system (Table 6).

CONCLUSION

Herein, GO-based new nanocomposites were synthesized and characterized using different standard analytical techniques to utilize them in raw leather tanning processes. FT-IR and SEM analysis data confirmed the successful formation of GO-based TiO_2 nanocomposite materials. XRD study provided crystalline and morphological characteristics of synthesized Graphene Oxide (GO), GO-TiO_2 (GT) and GO-PEG-TiO_2 (GPT) materials. The results of the DLS analysis showed the distribution and average particle sizes of GO, GT, and GTP which were 369 nm, 390 nm, and 432 nm respectively. These new nanocomposites [GO-TiO_2 (GT) and GO-PEG-TiO_2 (GPT)] have been successfully applied in the leather manufacturing process and they were found to work efficiently as potential tanning agents. The FESEM images of GO-TIO_2 and GO-TiO_2-PEG nanocomposites tanned leather revealed the successful penetration and bonding between leather fibres and composites functionalities. Different physico-mechanical tests such as shrinkage temperature, tensile strength, stitch strength, tear strength, flexing endurance, and crack resistance were carried out on the leathers processed with new nanocomposites. The shrinkage temperatures (Ts) of leathers tanned with GO-TiO_2 and GO-TiO_2-PEG composites ranged from 90 to 95 ^oC and 90 to 100 ^oC respectively which were consistent with the conventional chrome-tanned leather (control method). Thermogravimetric analyses of nanocomposites-tanned leathers showed characteristic patterns of degradation at higher temperatures which were highly comparable to those observed in the chrome-tanned leathers. The tensile strength of leathers tanned with the 6% nanocomposite materials was found to be 228 and 233 kg/cm respectively whereas this value was observed as 223 kg/cm in chrome-tanned leather. The maximum stitch tear strength of 6% GO-TiO_2-PEG composites tanned leather was found as 122 kg/cm which was significantly higher than the corresponding value of chrome-tanned leather (107 kg/cm). On the other hand, the magnitudes of total dissolved solids (TDS), total suspended solids (TSS), chemical oxygen demand (COD), and biochemical oxygen demand (BOD) found in wastewater generated from the leather tanning processes with both nanocomposites were significantly lower than those observed in the conventional chrome-tanned liquors. Maximum 90% TDS, 91% TSS, 70% COD and 75% BOD can be reduced by using 2% GO-TiO_2 nanocomposites in leather manufacturing whereas those values were found as 85%, 89%, 60% and 75% in the case of 2% GO-TiO_2-PEG nanocomposites. Pollution analysis data revealed that applications of new nanocomposites in raw leather tanning processes significantly reduced the toxicity and contamination in wastewater generated from leather industries. This novel approach of treating raw leathers with new nanocomposites is truly impressive and eco-friendly as these nanocomposite tanning agents successfully minimized the pollution load in the tannery wastewater stream and

worked more efficiently in comparison to those observed in conventional chrome tanning systems. Therefore, these new nanocomposite materials could be an efficient and viable alternative to traditional chrome tanning agents, which can potentially be used in leather manufacturing processes in various tannery industries for minimizing environmental pollution as well as to produce good quality leather products.

Author Contributions

Conceptualization – Mottalib MA, Chakma S; methodology – Mottalib MA, Chakma S, Biswas P; formal analysis – Biswas P, Chowdhury F; investigation – Biswas P, Chakma S, Chowdhury F; resources – Mottalib MA; writing-original draft preparation – Chakma S, Biswas P; writing-review and editing – Mottalib MA, Abdulll-Al-Mamun M, Goni MA; visualization – Chakma S, Biswas P; supervision – Mottalib MA, Chakma S. All authors have read and agreed to the published version of the manuscript.

Conflicts of Interest

The authors declare no conflict of interest.

Funding

This research received no external funding.

Acknowledgements

The authors gratefully acknowledge the laboratory facilities and bench space offered provided by the Institute of Leather Engineering and Technology (ILET), University of Dhaka and the Leather Research Institute, Bangladesh Council of Scientific and Industrial Research (BCSIR).

REFERENCES

[1] Shan H, Zeng C, Zhao C, Zhan H. Iron oxides decorated graphene oxide/chitosan composite beads for enhanced Cr(VI) removal from aqueous solution. International Journal of Biological Macromolecules. 2021; 172:197–209. https://doi.org/10.1016/j.ijbiomac.2021.01.060

[2] Bayisa YM, Bullo TA, Akuma DA. Chromium removal from tannery effluents by adsorption process via activated carbon chat stems (Catha edulis) using response surface methodology. BMC Research Notes. 2021; 14:431. https://doi.org/10.1186/s13104-021-05855-7

[3] Pradeep S, Sundaramoorthy S, Sathish M, Jayakumar GC, Rathinam A, Madhan B, Saravanan P, Rao JP. Chromium-free and waterless vegetable-aluminium tanning system for sustainable leather manufacture. Chemical Engineering Journal Advances. 2021; 7:100108. https://doi.org/10.1016/j.ceja.2021.100108

[4] Nashy EL-Shahat HA, Eid KA. High exhaustion of chrome tan, enhancement of leather properties and reduction of chrome tanning effluent impact. Egyptian Journal of Chemistry. 2019; 62(3):415-428. https://doi.org/10.21608/ejchem.2018.4393.1387

[5] Jannat N, Nahar H, Khan NS, Tanmoy MA, Mottalib MA, Goni MA, Khan M, Miran MS. Potential removal of chromium from tannery wastewater by water hyacinth roots. Water Conservation Science and Engineering. 2023; 8:21. https://doi.org/10.1007/s41101-023-00196-x

[6] Bithi SJ, Mottalib MA, Hijmun-Nahar, Miran MS, Ehsan MF, Rahman MM. Removal of Cr(VI) from wastewater by impregnated activated carbon generated from vegetable tanned leather waste with aluminium oxide. Results in Surfaces and Interfaces. 2024; 14:100197. https://doi.org/10.1016/j.rsurfi.2024.100197

[7] Moges A, Nkambule TTI, Fito J. The application of GO-Fe_3O_4 nanocomposite for chromium adsorption from tannery industry wastewater. Journal of Environmental Management. 2022; 305:114369. https://doi.org/10.1016/j.jenvman.2021.114369

[8] Zhou R, Jin Y, Lai S, Shi L, Bai L, Peng Z. A novel composite retanning system based on pH-responsive hydrogen bonding and hydrophobic interaction for cleaner leather processing. Journal of Cleaner Production. 2022; 339:130666. https://doi.org/10.1016/j.jclepro.2022.130666

[9] Wahiduzzaman M, Islam MM, Sikder AHF, Parveen Z. Bioaccumulation and heavy metal contamination in fish spe-cies of the Dhaleswari river of Bangladesh and related human health implications. Biological Trace Element Research. 2022; 200:3854-3866. https://doi.org/10.1007/s12011-021-02963-0

[10] Genawi NM, Ibrahim MH, El-Naas MH, Alshaik AE. Chromium removal from tannery wastewater by electrocoagulation: optimization and sludge characterization. Water. 2020; 12(5):1374. https://doi.org/10.3390/w12051374

[11] Kumar M, Maurya NS, Singh A, Rai MK. Efficient removal of Cr(VI) from aqueous solution by using tannery by-product (buffing dust). Heliyon. 2023; 9(4):e15038. https://doi.org/10.1016/j.heliyon.2023.e15038

[12] Daneshvar E, Zarrinmehr MJ, Kousha M, Hashtjin AM, Saratale GD, Maiti A, Vithanage M, Bhatnagar A. Hexavalent chromium removal from water by microalgal-based materials: adsorption, desorption and recovery studies. Bioresource Technology. 2019; 293:122064. https://doi. org/10.1016/j.biortech.2019.122064

[13] Braver-Sewradj SPD, Benthem JV, Staal YC, Ezendam J, Piersma AH, Hessel EV. Occupational exposure to hexavalent chromium. Part II. Hazard assessment of carcinogenic effects. Regulatory Toxicology and Pharmacology. 2021; 126:105045. https://doi.org/10.1016/j.yrtph.2021.105045

[14] Arellano-Sánchez MG, Devouge-Boyer C, Hubert-Roux M, Afonso C, Mignot M. Chromium determination in leather and other matrices: a review. Critical Reviews in Analytical Chemistry. 2022; 52(7):1537–1556. https://doi.org/10.1080/10408347.2021.1890545

[15] Eid MA, Nashy EHA, Eid KA, EI Ashkar EA, Borai E. Speciation of chromium ions in tanning effluents and subsequent determination of Cr (VI) by ICP-AES. Journal of the American Leather Chemists Association. 2002; 97(11):451-455.

[16] Fito J, Abewaa M, Nkambule T. Magnetite-impregnated biochar of parthenium hysterophorus for adsorption of Cr(VI) from tannery industrial wastewater. Applied Water Science. 2023; 13:78. https://doi.org/10.1007/s13201-023-01880-y

[17] Nure JF, Nkambule TTI. The recent advances in adsorption and membrane separation and their hybrid technologies for micropollutants removal from wastewater. Journal of Industrial and Engineering Chemistry. 2023; 126:92-114. https://doi.org/10.1016/j.jiec.2023.06.034

[18] Masuku M, Jemal F, Atagana HI, Hlongwa NW, Nkambule TTI. Advancing the development of nanocomposite adsorbent through zinc-doped nickel ferrite-pinecone biochar for removal of chromium (VI) from wastewater. Science of The Total Environment. 2023; 908:168136. https://doi.org/10.1016/j.scitotenv.2023.168136

[19] Fito J, Kefeni KK, Nkambule TTI. The potential of biochar-photocatalytic nanocomposites for removal of organic micropollutants from wastewater. Sci Total Environ. 2022; 829:154648. https://doi.org/10.1016/j.scitotenv.2022.154648

[20] Chen W, Chen Z, Long Z, Shan Z. Development of aldehyde and similar-to-aldehyde tanning agents. Textile Research Journal. 2021; 92(17-18):3387-3397. https://doi.org/10.1177/00405175211023813

[21] El-Wahab AH, El-Monem AF, Naser AM, Hussain AI, Nashy EHA, Lin L. Novel tanning agent based on silica-nano composite emulsion polymers. Pigment & Resin Technology. 2020; 49(4):283–294. https://doi.org/10.1108/PRT-12-2019-0113

[22] El-Monem AF, Hussain AI, Nashy EHA, El-Wahhab AH, Naser AM. Nanoemulsion based on acrylic acid ester co-polymer derivatives as an efficient pre-tanning agent for buffalo hide. Arabian Journal of Chemistry. 2017; 10(2):S3861-S3869. https://doi.org/10.1016/j.arabjc.2014.05.024

[23] Ibrahim AA, Youssef MSA, Nashy SHA, Eissa MM. Using of hyperbranched poly (amidoamine) as pre-tanning agent for leather. International Journal of Polymer Science. 2013; 120656. https://doi.org/10.1155/2013/120656

[24] El-Monem FA, Hussen AI, El-Wahab HA, Nashy EHA, Naser AM. Retanning agent for chrome tanned leather based on modern technique of emulsion polymers. Egyptian Journal of Chemistry. 2021; 64(1):503-516. https://doi.org/10.21608/ejchem.2020.29577.2636

[25] Lyu B, Gao J, Ma J, Gao D, Wang H, Han X. Nanocomposite based on erucic acid modified montmorillonite/sulfited rapeseed oil: preparation and application in leather. Applied Clay Science. 2016; 121-122:36-45. https://doi.org/10.1016/j.clay.2015.12.021

[26] Chen W, Zhang X, Mamadiev M, Zhao C, Wang Z, Xu H. Synthesis of interstratified graphene/montmorillonite composite material through organics-pillared, delamination and co-stacking and its application in hexavalent chromium removal from aqueous solution. Advanced Powder Technology. 2017; 28(2):521-533. https://doi.org/10.1016/j.apt.2016.10.021

[27] Lv S, Zhou Q, Li Y, He Y, Zhao H, Sun S. Tanning performance and environmental effects of nanosized graphene oxide tanning agent. Clean Technologies and Environmental Policy. 2016; 18:1997-2006. https://doi.org/10.1007/s10098-016-1128-9

[28] Ding W, Yi Y, Wang YN, Zhou J, Shi B. Preparation of a highly effective organic tanning agent with wide molecular weight distribution from bio-renewable sodium alginate. Chemistry Select. 2018; 3(43):12330-12335. https://doi.org/10.1002/slct.201802540

[29] Nashy EHA, Hussien AI, Essa MM. Novel retanning agents for chrome tanned leather based on emulsion–nano particles of styrene / butyl acrylate copolymers. Journal of American Leather Chemical Association. 2011; 106(9):241-248.

[30] Nashy EHA, Hussien AI, Essa MM. Synthesis and application of methyl meth-acrylate/butyl acrylate copolymers nano-emulsion as efficient re-tanning and lubricant agents for chrome tanned leather. Journal of Applied Polymer Science. 2011; 124(4):3293-3301. https://doi.org/10.1002/app.35208

[31] Liu K, Chen L, Chen Y, Wu J, Zhang W, Chen F, Fu Q. Preparation of polyester/reduced graphene oxide composites via in situ melt polycondensation and simultaneous thermo-reduction of graphene oxide. Journal of Materials Chemistry. 2011; 21(24):8612-8617. https://doi.org/10.1039/C1JM10717H

[32] Pan H, Wang S, Wang X, Gong C, Ding T. Synergistic effects of hydrophilic nano-SiO_2/graphene oxide @ copolymer nanocomposites in tanning leather. Advanced Powder Technology. 2020; 31(9):3910-3920. https://doi.org/10.1016/j.apt.2020.07.029

[33] Pendolino F, Armata N. Graphene oxide in environmental remediation process. Switzerland: Springer; 2017. 5-21 p. https://doi.org/10.1007/978-3-319-60429-9

[34] SATRA TM17, Shrinkage temperature of leather, SATRA Technology Centre, Northamptonshire. 1997.

[35] IULTCS/IUP 6, Leather - Physical and mechanical tests -Determination of tensile strength and percentage elongation, Geneva, Switzerland, 2020.

[36] DIN 53329, Testing of leather and artificial leather; tear growth test, German Institute for Standardization. 1982.

[37] SATRA PM-162, Tear strength - Baumann method, SATRA Technology Centre, Northamptonshire. 2017.

[38] IULTCS/IUP 9, Leather - Determination of distension and strength of surface (Ball burst method). 2015.

[39] SATRA PM-55, Flexing resistance of upper materials - Bally flexometer, SATRA Technology Centre, Northamptonshire. 1999.

[40] Hossain MD, Azam FA, Chowdhury M. Quality assessment of shoe leather based on the properties of strength and comfort, collected from different footwear and leather industries in Bangladesh. Textile & Leather Review. 2021; 4(1):30-37. https://doi.org/10.31881/TLR.2020.20

[41] DoE, The Environment Conservation Rule, 1997, Bangladesh.

[42] He D, Peng Z, Gong W, Luo Y, Zhao P, Kong L. Mechanism of a green graphene oxide reduction with reusable potassium carbonate. RSC advances. 2015; 5(16):11966-11972. https://doi.org/10.1039/C4RA14511A

[43] Ferrari AC, Robertson J. Interpretation of raman spectra of disordered and amorphous carbon. Physical Review B. 2000; 61(20):14095. https://doi.org/10.1103/PhysRevB.61.14095

[44] Shin DS, Kim HG, Ahn HS, Jeong HY, Kim YJ, Odkhuu D, Tsogbadrakh N, Kim BH. Distribution of oxygen functional groups of graphene oxide obtained from low-temperature atomic layer deposition of titanium oxide. RSC Advances. 2017; 7(23):13979-13984. https://doi.org/10.1039/C7RA00114B

[45] Kumar N, Das S, Bernhard C, Varma GD. Effect of graphene oxide doping on superconducting properties of bulk MgB_2. Superconductor Science and Technology. 2013; 26(9):095008. https://doi.org/10.1088/0953-2048/26/9/095008

[46] Wang C, Feng L, Yang H, Xin G, Li W, Zheng J, Tian W, Li X. Graphene oxide stabilized polyethylene glycol for heat storage. Physical Chemistry Chemical Physics. 2012; 14(38):13233-13238. https://doi.org/10.1039/C2CP41988B

[47] Hu X, Yu Y, Hou W, Zhou J, Song L. Effects of particle size and pH value on the hydrophilicity of graphene oxide. Applied Surface Science. 2013; 273:118-121. https://doi.org/10.1016/j.apsusc.2013.01.201

[48] Nayak C, Nigam S, Pandey M, Sudarsan V, Majumder C, Jha SN, Bhatacharyya D, Vatsa RK, Kshirsagar RJ. Nano-size effects on the nature of bonding in $Y_2Sn_2O_7$: EXAFS and Raman spectroscopic investigations. Chemical Physics Letters. 2014; 597:51-56. https://doi.org/10.1016/j.cplett.2014.02.028

[49] Paul G, Verma S, Jalil O, Thakur D, Pandey CM, Kumar D. PEDOT: PSS-grafted graphene oxide-titanium dioxide nanohybrid-based conducting paper for glucose detection. Polymers for Advanced Technologies. 2021; 32(4):1774-1782. https://doi.org/10.1002/pat.5213

[50] Yorgancioglu A, Onem E, Yilmaz O, Karavana HA. Interactions betwe en collagen and alternative leather tanning systems to chromium salts by comparative thermal analysis methods. Johnson Matthey Technology Review. 2022; 66(2):215-226. https://doi.org/10.1595/205651322X16225583463559

[51] Liu J, Luo L, Hu Y, Wang F, Zheng X, Tang K. Kinetics and mechanism of thermal degradation of vegetable-tanned leather fiber. Journal of Leather Science and Engineering. 2019; 1:9. https://doi.org/10.1186/s42825-019-0010-z